Solid state characterization of a 5´-*O*-oxalatoyl prodrug of zidovudine (azidothymidine)

Diego E. Kassuha,[1,2] Flavia P. Bruno,[1,3] Gustavo A Monti,[4] Norma R. Sperandeo[1*]

[1]Universidad Nacional de Córdoba. Facultad de Ciencias Químicas. Departamento de Ciencias Farmacéuticas and UNITEFA-CONICET. Haya de la Torre y Medina Allende, Ciudad Universitaria, X5000HUA, Córdoba, Argentina.

[2]Present address: Instituto de Investigaciones en Ciencias Químicas. Facultad de Ciencias Químicas y Tecnológicas. Universidad Católica de Cuyo, San Juan, Argentina.

[3]Present address: Laboratorio Fresenius Kabi, Del Comercio 757, X5016JSA Córdoba, Argentina.

[4] Universidad Nacional de Córdoba. Facultad de Astronomía, Matemática, Física y Computación. -IFEG-CONICET, Ciudad Universitaria, X5000HUA Córdoba, Argentina.

•**Corresponding author:** Prof. Dr. Norma R. Sperandeo, e-mail: nrscor@fcq.unc.edu.ar

TE: +54 351 5353865.

Abstract

The importance of polymorphism in pharmaceuticals makes its study relevant. The aim of this study was to investigate the solid-state forms in which 3´-azido-2´,3´-dideoxi-5´-O-oxalatoyl-thymidinic acid (AZT-Ac), a zidovudine (AZT) prodrug with improved pharmacokinetic properties, may exist. Samples were prepared using different crystallization conditions, and characterized using powder X-ray diffraction, solid state nuclear magnetic resonance, differential scanning calorimetry, thermogravimetry and hot stage microscopy. Pharmaceutical relevant properties such as solid-state stability and intrinsic dissolution rate (IDR) at 37 °C in simulated gastric fluid (SGF) were also evaluated. AZT-Ac was found able to exist as a crystalline polymorph (AZT-Ac-C) and an amorphous phase (AZT-Ac-A), which were thoroughly characterized. At 40 °C/75% RH, AZT-Ac-A in part devitrified to AZT-Ac-C, and partially hydrolyzed to AZT after 7 and 14 days of storage, respectively. AZT-Ac-C was physically stable at 40 °C/75% RH but partly hydrolyzed to AZT after 14 days of storage. In SGF, AZT-Ac-C exhibited a linear ID profile and provided an ID rate of 0.494 mg/min/cm^2 while AZT-Ac-A exhibited a nonlinear profile. Therefore, the crystalline form demonstrated advantages over the amorphous one in terms of solid state stability and IDR, but approaches to enhance its stability should be considered for further formulation of this prodrug.

Keywords: crystallization, differential scanning calorimetry, drugs, Nuclear Magnetic Resonance, nucleoside inhibitors, X-ray diffraction.

1. **Introduction**

Zidovudine (azidothymidine) (AZT, Figure 1a) was the first active pharmaceutical ingredient to be approved by the Food and Drug Administration for the treatment of Acquired Immunodeficiency Syndrome (AIDS) in humans, and is still in use as part of the highly active antiretroviral therapy (HAART) regimen (Shey et al., 2013). Although its efficacy has long been demonstrated, AZT has various unfavorable aspects that constitute major concerns, such as cellular toxicity (D'Andrea et al., 2008) and suboptimal pharmacokinetic properties (Barbier et al., 2000; Narciso et al., 2014; Eilers et al., 2008). Among the clinical circumstances of AZT toxicity there are numerous hematological effects, suppression of bone marrow cell functions, liver disorders, myopathies, etc. (Khandazhinskaya and Shirokova, 2013). In addition, AZT exhibits short plasma half-life ($t_{1/2} \approx 1$ h) (Barbier et al., 2000), low plasma protein-binding capacity (Narciso et al., 2014) and incapacity to reach effective concentrations in viral reservoir tissues (Eilers et al., 2008). For this reason, AZT has to be administered frequently and at high doses, thereby increasing the incidence of unwanted side effects that often compromised the adherence of the patient to the anti-HIV treatment (Narciso et al., 2014; Quevedo and Briñón, 2009).

Several strategies have been applied in order to enhance the oral bioavailability of AZT as well as to prolong its elimination half-life (De Clercq, 2007), with the preparation of prodrugs being a widely applied methodology (D'Andrea et al., 2008; Khandazhinskaya and Shirokova, 2013; Quevedo and Briñón, 2009; Dalpiaz et al., 2012; Moroni et al., 2002; Parang et al., 2000; Quevedo et al., 2008; Raviolo et al., 2009; Solyev et al., 2012; Ribone et al., 2016). Among these prodrugs, 3´-azido-2´,3´-deoxy-5´-O-oxalatoyl-thymidine (AZT-Ac, Figure 1b) exhibited anti-HIV potency, low cytotoxicity and improved *in vitro* permeability. In fact, it permeates the rat intestinal segment at a lower rate than AZT, but resists enzymatic hydrolysis with no evidence of saturable transport mechanisms in the

jejunum or the proximal ileum (as the case of AZT) and, has an extended plasma half-life in rats (Quevedo and Briñón, 2009). AZT-Ac also displayed high stability under acidic conditions (pH 2) for 48 h, and suffered hydrolysis at pH 7.2 but its calculated $t_{1/2}$ was 12.8 h (Ribone et al., 2016).

Considering that AZT-Ac is a prodrug of AZT with improved hydrolytic and pharmacokinetic properties, and that thymidine nucleosides such as AZT and stavudine exhibit crystalline polymorphism (Gandhi et al., 2000; Soares et al., 2013), the goal of this study was to investigate the existence of different polymorphs of AZT-Ac in order to support the development effort. To this aim, we subjected AZT-Ac to a polymorph screen using several solid form screening techniques. We isolated only two solid forms, which were characterized by means of powder X-ray diffraction (PXRD), solid state nuclear magnetic resonance (SS ^{13}CNMR), differential scanning calorimetry (DSC), thermogravimetry (TG) and hot-stage microscopy (HSM). The effects of temperature and moisture on the chemical and physical stabilities of both solid forms of AZT-Ac were investigated at 40 °C/75% relative humidity (RH) along with their disc intrinsic dissolution behavior in simulated gastric fluid without pepsin at 37 °C in order to compare their solid state stabilities and dissolution behaviors.

2. Material and methods

2.1 Materials

AZT was generously provided by Filaxis Laboratories (Buenos Aires, Argentina). AZT-Ac raw material (AZT-Ac-r) was synthesized and purified following a described procedure (Moroni et al., 2002). Precoated silica gel 60 F254 plates (Merck KGaA, Germany), filter paper (2.7 μm, Whatman 542, UK) and nylon membranes (0.45 μm, Pall Corporation, USA) were commercially acquired. All the solvents used were of analytical

grade, and Milli-Q® water (Millipore, Bedford, USA) was also utilized. For thin layer chromatography (TLC) analyses, ethyl acetate-acetone-methanol 5:3:2 v/v, and pre-coated plates of silica gel 60 F254 (Merck Chemicals) were used as the eluting solvent system and stationary phase, respectively. Spots were visualized with UV light and iodide vapors.

2.2 Preparation of AZT-Ac forms

In search of different polymorphs for AZT-Ac a variety of solid form screening techniques were used, which included crystallization (slow and fast) from solution, antisolvent precipitation, vapor diffusion crystallization (Cunha, 2008), polymer induced heteronucleation (Price et al., 2005) and lyophilization (Kassuha et al., 2015). Samples generated by these techniques were initially analyzed by means of TLC for chemical purity, finding that they were chromatographically pure, as no other spots than that of AZT-Ac were detected. Eventually, only two different solid forms were obtained, which will be reported in this paper. These two forms were named hereafter as AZT-Ac-C and AZT-Ac-A, and were reproducibly obtained using the following procedures:

AZT-Ac-C: a saturated solution of AZT-Ac-r was prepared in acetonitrile at 20-25 °C (RT), filtered (Whatman 532 paper) into a beaker. The beaker was covered with filter paper and allowed to evaporate at room temperature (RT, 20-25 °C) in the dark. Then, the isolated crystals were stored in a desiccator under $CaCl_2$.

AZT-Ac-A: a *t*-butanol-water (20:80, v/v) solution of AZT-Ac-r (30 mg/mL) was frozen in air liquid and lyophilized at -40 °C for 24 h (Freezone 6, Labconco®, USA). The resultant solid was subjected to a secondary drying in a desiccator (vacuum, RT, P_2O_4) for 24 h and stored at -20 °C in a tightly closed vial till analyzed.

2.3 PXRD

PXRD patterns were collected at RT on a X´PERT PRO X-ray diffractometer (PANalytical, The Netherlands) fitted with a Copper tube (Cu Kα = 1.54178 Å) and a Ni filter, with the X-ray generator being set at a voltage of 40 kV and a current of 30 mA. Samples were analyzed with a step size of 0.05° 2θ and a step time of 3 s from 3 to 35° 2θ, using a 25 mm diameter Si single crystal holder.

2.4 SS ^{13}CNMR

SS ^{13}CNMR spectra were recorded at room temperature [Bruker Avance II spectrometer operating at 300.13 MHz (protons) and 75.47 MHz (carbons), equipped with a 4 mm MAS probe] using the CP/MAS sequence with proton decoupling during acquisition. Adamantane was used as an external reference for the ^{13}C spectra and to set the Harmann−Hahn matching condition in the cross-polarization experiments. The spinning rate, recycling time, contact time during CP and the acquisition time were 9 kHz, 30 s, 2 ms and 41 ms, respectively. The numbers of transients were 256 and the SPINAL 64 sequence was used for decoupling during acquisition with the proton decoupling field H_{1H} satisfying $\omega_{1H}/(2\pi) = \gamma H_{1H}/(2\pi) = 78$ kHz. The quaternary carbon edition spectra was acquired with the non-quaternary suppression (NQS) sequence, with the ^{1}H and ^{13}C radio frequency fields being removed during 40 μs after CP and before the acquisition. This delay allowed the carbon magnetization to decay because of ^{1}H−^{13}C dipolar coupling, resulting in spectra where CH and CH_2 were substantially removed. Assignment of the ^{13}C resonances was accomplished with the aid of NQS experiments and residual dipolar coupling in the solid-state and by comparison with the ^{13}C spectrum (DMSO-d_6) of AZT-Ac-r.

147 2.5 DSC, TG and HSM

148 DSC and TG measurements were recorded on MDSC 2920 and TG 2950 analyzers (TA
149 Instruments Inc., USA), respectively. Samples (1-2 mg) were heated in non- hermetically
150 sealed aluminum pans, using a heating rate of 10 °C/min and a nitrogen (99.99 %) purge of 50
151 mL/min. The DSC and TG temperature axes were calibrated with indium (99.99 %,
152 *m.p.*156.60 °C) and the Curie point of Ni (358.14 °C), respectively. Empty aluminum pans
153 were used as references. Data were analyzed using the Universal Analysis 2000 software (TA
154 Instruments Inc.). The physical and morphological changes that occurred in the samples
155 during heating were observed through a microscope fitted with a Kofler hot stage (Leitz,
156 Wetzlar, Germany) at a constant rate of 8 °C/min.

157

158 2.6 Solid-state stability

159 To investigate the effect of storage temperature and moisture on the physical and
160 chemical stabilities of the samples, 200 mg of each solid form (n= 2) were stored at 40
161 °C/75% RH (open glass vials inside a drying pistol (ISV, Argentina) filled with a saturated
162 aqueous solution of NaCl) and analyzed via TLC and PXRD at various time intervals to
163 evaluate chemical purity and phase changes.

164

165 2.7 Disc intrinsic dissolution measurements

166 Intrinsic dissolution experiments were performed using a rotating disc apparatus that
167 meets USP specifications (USP, 2012) on a Hanson SR6 dissolution tester (Hanson Research,
168 Chatsworth, CA). Powdered samples (100.0 mg) of AZT-Ac-C and AZT-Ac-A were directly
169 compacted into the stainless steel cylinder of the rotating disc apparatus (resulting in discs at
170 one side of the cylinder with surface area of 0.5 cm^2) at 118 MPa (dwell time of 1 min), a
171 compromise compression that produced non-disintegrating discs and did not induce

polymorphic transitions and devitrification, as indicated by PXRD analyses. Disc intrinsic dissolution was carried out at 50 rpm in 250 mL of degassed SGF without pepsin at 37 ± 0.5°C. This medium and its volume was established by considering the chemical stability of AZT-Ac in acidic media (Ribone et al., 2016), its solubility (~8 mg/mL, pH 1.2 at 37 °C), and the minimum volume required to completely immerse the die. The 250 mL volume maintained sink conditions during the experiment (since the concentrations of AZT-Ac-C and AZT-Ac-A after 25 min were 0.028 and 0.035 mg/mL respectively) and completely immersed the die. Therefore, the concentrations applied in the experiments were below 0.8 mg/mL (10 % of the saturation concentration). Aliquots of 5 mL were withdrawn (with replacement) at time intervals of 5, 10, 15, 20 and 25 min, filtered (0.45 µm), and analyzed by UV spectroscopy at 267 nm. In all cases, the first mL was discarded. Dissolution tests were performed in triplicate (AZT-Ac-A) and in duplicate (AZT-AC-C). For the quantification of the concentration of AZT-Ac in the dissolution medium, a standard curve was prepared using five concentration levels. The cumulative amount of dissolved test specimen per initial area was plotted against time. The intrinsic dissolution rate (or mass flux (***J***) in mg/cm^2/min) was calculated from the slope of the regression line (USP, 2012).

3. Results and discussion

3.1 Identification of AZT-Ac polymorphs

Figure 2 displays the powder patterns for the raw material (Figure 2a), AZT-Ac-C (Figure 2b) and AZT-Ac-A (Figure 2c). As shown in Figures 2a and 2b, the powder patterns of the raw material and AZT-Ac-C were coincident in the position of the diffraction peaks, and no additional reflections were visualized, indicating that they represented the same phase. In contrast, the powder pattern of AZT-Ac-A (Figure 2c) had a broad halo and an absence of diffraction peaks, revealing that it was X-ray amorphous.

It is worth of mention that the PXRD patterns of samples obtained by using other crystallization technique such as fast evaporation from different solvents; vapor diffusion crystallization with petroleum ether (35–60 °C) as antisolvent, and polymer induced heteronucleation were coincident (Figures not shown) to those of Figures 2a and 2b, indicating a low likelihood for several crystalline forms of AZT-Ac. Unfortunately, we could not obtain crystals suitable for resolving the crystalline structure of AZT-Ac-C, thus, in order to gain structural information on this form, its SS ^{13}CNMR spectrum was obtained (Figure 3).

As seen in Figure 3a, the spectrum of AZT-Ac-C exhibited well-resolved signals for the 11 carbons of the molecule (Figure 1b), with their line widths being all in the range of 30-50 Hz, indicating an ordered and crystalline form (Monti et al., 2014). The resonances at 83.3, 139.9, 149.9 and 166.9 ppm showed a broadened and split structure but these effects were due to coupling to ^{14}N quadrupolar nuclei not due to the presence of more than one molecule in the asymmetric unit of AZT-Ac, which thus comprised one molecule of AZT-Ac. In particular, the resonances at 83.5, 139.9 and 166.9 ppm consisted of two lines with relative intensities of 2:1, which is typical of ^{13}C nuclei coupled to a single ^{14}N (Olivieri et al., 1988). Thus, these were assigned to C1´, C6 and C4 respectively (Figure 1b, Table S1). In contrast, the resonance at 149.9 ppm consisted of four lines, which is characteristic of a ^{13}C nucleus coupled to a pair of ^{14}N (Olivieri et al., 1988); hence, this resonance was assigned to C2 (Table S1). According to the NQS spectrum (Figure 3b), the quaternary carbons of AZT-Ac-C resonated at 110.7 (C5), 149.9 (C2), 157.5 (C1´´), 159.1 (C2´´), and 166.9 ppm (C4) (Table S1), and it is worth mentioning that the methine carbons (C2´ and C5´´) were also observed in the NQS spectrum (Figure 3b) because their resonance intensities were severe affected but not totally suppressed during the delay time. C1´ (83.5 ppm) and C4´ (82.9 ppm) (Table S1) were assigned without ambiguity, as the C1´ resonance line shape revealed a residual dipolar

interaction structure due to bonding of C1´ to N1 while the one of C4´ did not. In the case of C3´ (59.1 ppm), no residual dipolar coupling was observed, probably due to the mobility of the azide group or the puckering motion of the furanose ring (Kolodziejski and Klinowski, 1999), which can contribute to averaging out the coupling.

3.2 DSC, TG and HSM

The behavior on heating of AZT-Ac-C and AZT-Ac-A was investigated by DSC and TG (Figure 4). The DSC curve of AZT-Ac-C (Figure 4a) exhibited, in the 25-160 °C temperature range, an endotherm at 92.1 °C (extrapolated onset temperature), followed by several small broad endothermic effects. According to the TG data (Figure 4a), the endotherm at 92.1 °C was associated with weight loss, suggesting that the sample melted with decomposition. The interpretation of the DSC events just described was assisted by HSM and TLC. Microscopic observations revealed that the transparent prismatic particles (Figure S1, Supplementary material) of AZT-Ac-C (not embebbed in silicon oil in order to provide experimental conditions similar to those in the DSC and TG experiments) melted at about 93 °C and upon further heating, the molten phase diminished in size and became brownish, a typical feature of a decomposition process (Sperandeo and de Bertorello, 2001; Sperandeo et al., 2005; Cuffini et al., 2007; Bruno et al., 2010). TLC analysis of the obtained residue confirmed the decomposition of the sample as several spots were detected, with AZT-Ac being absent.

The DSC curve of AZT-Ac-A (Figure 4b) showed, in the 25-110 °C temperature range, only a very broad endotherm at 48.5 °C (Tpeak), resembling a glass transition overlapped with a desolvation process (Kassuha et al., 2015) as the sample was X-ray amorphous and the respective TG curve (Figure 4b) exhibited a gradual weight loss. Taking into account that AZT-Ac-A was obtained by lyophilization from *t*-butanol-water and both

solvents can remain in lyophilized solids, as it was observed for other lyophilized samples (Kassuha et al., 2015; Teagarden and Baker, 2002), the occurrence of a desolvation process was considered. Above 110 °C, the DSC curve displayed another very small broad endotherm superimposed with a large exothermic effect that continued at temperatures above 170 °C. Both effects had associated a TG weight loss (Figure 4b´) that continued above 170 °C, typical of a decomposition process that continued at higher temperatures (Sperandeo and de Bertorello, 2001; Cuffini et al., 2007; Bruno et al., 2010). Thus, AZT-Ac-A was visually examined by HSM to assist in the interpretation of the DSC events. Heating the white opaque particles (Figure S1, Supplementary material) of AZT-Ac-A (not immersed in silicon oil) from 25° C revealed that they became almost colorless and compacted at about 60 °C, which was consistent with a glass transition concomitant with a desorption process. The sample started to move (at about 80 °C), became liquefied (at about 103 °C) and on further heating, the molten phase diminished in size and brownish. TLC analysis of the obtained residue confirmed the decomposition of the sample as the AZT-Ac spot was not detected. Further studies using other analytical techniques should be necessary to determine the glass transition temperature of AZT-Ac-A as well as to identify the residual solvents.

3.3 Solid-state stability

The solid-state stabilities of AZT-Ac-C and AZT-Ac-A were evaluated at 40 °C/75% RH. Exposure of AZT-Ac-C to the assayed conditions for 14 days did not result in polymorphic conversions as indicated by PXRD. In fact, the powder patterns of AZT-Ac-C (Figure 5a), collected after 7 and 14 days of storage at 40 °C/75% RH did not exhibit new reflections attributable to hydrate formation or polymorphic conversions. However, TLC analysis of an aliquot taken at day 14 revealed the presence of free AZT, indicating that the ester bond of AZT-Ac-C had partially hydrolyzed affording its parent compound; hence its

stability was not investigated further. It should be noted that the characteristic peaks of AZT could not be visualized in Figure 5a, suggesting that its quantity was below to the detection limit of PXRD (1-5%) (Pecharsky and Zavalij, 2003). In contrast, exposure of AZT-Ac-A to temperature and moisture provoked its devitrification to AZT-Ac-C as indicated by PXRD. Indeed, the XRD patterns registered at day 7 and 14 (Figure 5b) exhibited various low intensity peaks of AZT-Ac-C superimposed to the amorphous halo, indicating that AZT-Ac-A partly devitrified to its crystalline counterpart. In addition, TLC analyses revealed the presence of free AZT at day 14, indicating that the temperature and humidity promoted its hydrolysis to its parent compound. Therefore, AZT-Ac-C and AZT-Ac-A cannot be stored in the typical conditions of a hot and humid climate without any special storage and handling instructions.

3.4 Intrinsic dissolution behavior

Intrinsic dissolution is a pharmacopeial (USP, 2012; EP, 2013) method for the evaluation of drug powders and it has wide application in characterizing new chemical entities (NCE) during the formulation development since parameters which control the rate of dissolution such as surface area exposed to the medium, temperature, stirring rate, and pH, are kept constant (USP, 2012; Löbmann et al., 2014; Sehic et al., 2010; Kaplan, 1972). In addition, Kaplan (Kaplan, 1972) had suggested that intrinsic dissolution rates (*J*), determined in the 1-7 pH range at 50 rpm and 37 °C, may be useful to predict absorption problems as compounds with $J > 1$ mg/min/cm^2 are usually not prone to dissolution rate limited absorption; with $J < 0.1$ mg/min/cm^2 usually exhibit dissolution rate limited absorption, and with J between 0.1 and 1.0 mg/min/cm^2 are borderline compounds; thus, additional information would be required to ascertain the effect of dissolution on the absorption rate (Du et al., 2013).

297 The amounts released per initial compact area (mg/cm^2) of AZT-Ac-C and AZT-Ac-A
298 are shown in Figure 6. The profile of AZT-Ac-C (Figure 6a) was a typical linear intrinsic
299 dissolution plot (R^2> 0.999), indicating good linearity between time and amount released per
300 unit area. The intrinsic dissolution rate, calculated from the slope of the regression line, was
301 found to be 0.494 mg/min/cm^2. In contrast, the intrinsic dissolution profile of AZT-Ac-A was
302 not linear (Figure 6b), showing an upward curvature that is typical of experimental problems
303 such as physical degradation of the compact by cracking or erosion (USP, 2012). Regression
304 analysis of all the data points of AZT-Ac-A showed that quadratic fitting (*i.e.* second−order
305 polynomial) gave an excellent regression (R^2 > 0.9995). Thus, in order to estimate the
306 intrinsic dissolution rate *(J)* of AZT-Ac-A, linear regression analysis was performed on data
307 points in the initial linear region of the dissolution curve (i.e. up to 10 min, inset of Figure 6)
308 as recommended by the United States Pharmocopeia (USP, 2012), which provided and IDR
309 of 0.397 mg/min/cm^2. It is worth of mention that after the dissolution experiments, the dies
310 were patted dried and visually examined under a magnifying glass to evaluate if changes had
311 occurred on the surface of discs. No changes in the surface of the compacts of AZT-Ac-C
312 were detected after dissolution. In contrast, the compacts of AZT-Ac-A showed holes and
313 lines, indicating that the surface area of the discs did not remain constant during the assay,
314 and this make an estimate of its IDR speculative at best.
315 According to Kaplan's classification (Kaplan, 1972; Du et al., 2013; Yao et al., 2014),
316 AZT-Ac belonged to the category of borderline NCE as the *J* values of AZT-Ac-C and AZT-
317 Ac-A were between 0.1 and 1.0 mg/min/cm^2. Hence, additional information may be required
318 to ascertain the effect of dissolution on the absorption rate of AZT-Ac.

319 **Conclusions**

320 This investigation contributes to the preformulation assessment of AZT-Ac by
321 exploring some aspects of its solid state properties and inherent stability. Two solid forms of

AZT-Ac were prepared and physically characterized by PXRD, SSNMR, DSC, TG and HSM. Although the enzymatic and stability of AZT-Ac in solution it was found good, especially in acidic conditions (Ribone et al., 2016), our research studies demonstrated that under hot and humid climate conditions (40°C/75% RH), the solid state stability of AZT-Ac is not good as its two solid forms partly hydrolyzed to the parent compound AZT after 14 days of storage. In addition, AZT-Ac-A devitrified partially to the crystalline form after 7 days of storage, suggesting that the amorphous form was not optimal to use for further development. The ID rates of AZT-Ac-C and AZT-Ac-A were determined to fall in the range 0.1- 1.0 mg/cm^2/min, which suggested that this prodrug could exhibit dissolution rate limited absorption. Therefore, approaches to enhance the solid state stability and dissolution rate of AZT-Ac-C should be considered in a further development.

Acknowledgements

This work was supported by SECyT-UNC and FONCyT of Argentina. FPB and DEK are grateful for financial support from the CONICET Type II Doctoral fellowships. DEK also thanks Secretaria de Ciencia, Técnica e Innovación (SeCiTI de San Juan (Argentina) for financial support. We thank Dr. P. Hobson, native speaker, for revision of the manuscript.

Declaration of interest: none.

References

Barbier O, Turgeon D, Girard C, Green MD, Tephly TR, Hum DW, et al. 3′-Azido-3′-deoxythymidine (AZT) is glucuronidated by human UDP-glucuronosyltransferase 2B7 (UGT2B7). Drug Metab Dispos, 2000; 28: 497–502.

Bruno FP, Caira MR, Monti GA, Kassuha DE, Sperandeo NR. Spectroscopic, thermal and X-ray structural study of the antiparasitic and antiviral drug nitazoxanide. J Mol Struct, 2010; 984: 51-57.

Cuffini S, Ayala A, Mendes Filho AJ, Ellena J, Mascarenhas Y, *et al.* Physicochemical Characterization of Deflazacort: Thermal Analysis, Crystallographic and Spectroscopic Study. Steroids, 2007; 72: 61-69.

Cunha S. Métodos Simples de Formação de Monocristal de Substância Orgânica para Estudo Estrutural por Difração de Raios X. Quim Nova 2008; 31: 906-909.

D'Andrea G, Brisdelli F, Bozzi A. AZT: an old drug with new perspectives. Curr Clin Pharmacol, 2008; 3: 20–37.

Dalpiaz A, Paganetto G, Pavan B, Fogagnolo M, Medici A, Beggiato S, *et al.* Zidovudine and ursodeoxycholic acid conjugation: design of a new prodrug potentially able to bypass the active efflux transport systems of the central nervous system. Mol Pharmaceut, 2012; 9: 957-968.

De Clercq E. The design of drugs for HIV and HCV. Nat Rev Drug Discov, 2007; 6 (12):1001-18.

Du W, Zhou Y, Gong Y, Zhao C. Investigation of physicochemical properties and in-vitro in-vivo evaluation of agomelatine polymorphs. Asian J Pharm Sci, 2013; 8: 181-190.

Eilers M, Roy U, Mondal D. MRP (ABCC) transporters-mediated efflux of anti-HIV drugs, saquinavir and zidovudine, from human endothelial cells. *Exp Biol Med,* 2008; 233: 1149–1160.

European Pharmacopoeia. 8th ed. Strasbourg: Council of Europe, 2013; 2.9.29, Intrinsic dissolution, 331-332.

Gandhi RB, Bogardus JB, Bugay DE, Perrone RK, Kaplan MA. Pharmaceutical relationships of three solid state forms of stavudine. Int J Pharm, 2000; 201: 221-237.

371 Kaplan SA. Biopharmaceutical considerations in drug formulation design and
372 evaluation. Drug Metab Rev, 1972; 1:15-33.
373 Kassuha D, Aiassa V, Bruno F, Cuadra G, Sperandeo N. Preparation and
374 characterization of polymorphs of the glucocorticoid deflazacort. Pharm Dev Technol, 2015;
375 20(4): 401-409.
376 Khandazhinskaya AL, Shirokova EA. AZT 5'-Phosphonates: Achievements and
377 Trends in the Treatment and Prevention of HIV Infection. Acta Naturae, 2013; 5(3): 54–61.
378 Kolodziejski W, Klinowski J. ^{13}C CP/MAS NMR study of anti-HIV-1 agent AZT.
379 Chem Phys Letters 1999; 303: 183-186. https://doi.org/10.1016/S0009-2614(99)00193-1
380 Löbmann K, Flouda K, Qiu D, Tsolakou T, Wang W, Rades T. The Influence of
381 Pressure on the Intrinsic Dissolution Rate of Amorphous Indomethacin. Pharmaceutics 2014;
382 6: 481-493.
383 Monti GA, Chattah AK, Garro Linck Y. Solid State Nuclear Magnetic Resonance in
384 Pharmaceutical Compounds. Annu Rep NMR Spectro, 2014; 83: 221-269.
385 Moroni GN, Bogdanov PM, Briñón MC. Synthesis and in vitro antibacterial activity
386 of novel 5-*O*-analog derivatives of zidovudine as potential prodrugs. Nucleos Nucleot Nucl,
387 2002; 21: 231-241.
388 Narciso P, Bolli A, Fasano M, Ascenzi P. Binding of Anti-HIV Drugs to Human
389 Serum Albumin. IUBMB Life, 2014; 56(10): 609–614.
390 Olivieri AC, Frydman L, Grasselli M, Días LE. Analysis of ^{13}C, ^{14}N residual dipolar
391 coupling in the ^{13}C CP/MAS NMR spectra of ribonucleosides. Magn Res Chem, 1988; 26:
392 281-286.
393 Parang K, Wiebe LI, Knaus EE. Novel approaches for designing 5-*O*-ester prodrugs
394 of 3-azido-2, 3-dideoxythymidine (AZT). Curr Med Chem, 2000; 7: 995-1039.

Pecharsky VK, Zavalij PY. Fundamentals of Powder Diffraction and Structural Characterization of Materials. Springer Science + Business Media, Inc. 2003, p. 389. ISBN 978-0-387-09579-0

Price CP, Grzesiak AL, Matzger AJ. Crystalline Polymorph Selection and Discovery with Polymer Heteronuclei. J Am Chem Soc, 2005; 127: 5512-5517.

Quevedo MA, Briñón MC. In Vitro and in Vivo pharmacokinetic characterization of two novel prodrugs of zidovudine. Antiviral Res, 2009; 1: 103-111.

Quevedo MA, Ribone SR, Moroni GR, Briñón MC.Binding to human serum albumin of zidovudine (AZT) and novel AZT derivatives. Experimental and theoretical analyses. Bioorg Med Chem, 2008; 16: 2779–2790.

Raviolo MA, Trinchero-Hernández JS, Turk G, Briñón MC. Synthesis and antiretroviral evaluation of novel derivatives of Zidovudine. J Braz Chem Soc, 2009; 20: 1870-1877.

Ribone, SR, Schenfeld, EM, Madrid M, Pierini AB, Quevedo MA. Evaluation and synthesis of AZT prodrugs with optimized chemical stabilities: experimental and theoretical analyses. New J Chem, 2016; 40, 2383-2392**.**

Sehic S, Betz G, Hadzidedi S, Kocova El-Arini S, Leuenberger H. Investigation of intrinsic dissolution behavior of different carbamazepine samples. Int J Pharm, 2010; 386: 77–90.

Shey MS, Kongnyuy EJ, Alobwede SM, Wiysonge CS. Co-formulated abacavir-lamivudine-zidovudine for initial treatment of HIV infection and AIDS. Cochrane Database Syst Rev, 2013; 28(3): 1-38.

Soares KC, Rediquieri CF, Souza J, Serra CH, Abrahamsson B, Groot DW, et al. Biowaiver monographs for immediate-release solid oral dosage forms: Zidovudine (azidothymidine). J Pharm Sci, 2013; 102: 2409-2423.

Solyev PN, Shipitsin AB, Karpenko IL, Nosik DN. Synthesis and Anti-HIV Properties of New Carbamate Prodrugs of AZT. Chem Biol Drug Des, 2012; 80: 947-952.

Sperandeo NR, de Bertorello MM. Solid state characterization of potential protozoocidal agents-aminoisoxazolyl napthoquinones. Thermochim Acta, 2001; 378, 67-71.

Sperandeo NR, Karlsson A, Cuffini S, Pagola S, Stephens PW. The Crystal Structure and Physicochemical Characteristics of 2-Hydroxy-N- [3(5)-pyrazolyl]-1,4-naphthoquinone-4-imine, a New Antitrypanosomal Compound. AAPS PharmSciTech, 2005; 6 (4): E655-E663.

Teagarden DL, Baker DS. Practical aspects of lyophilization using non-aqueous co-solvent systems. Eur J Pharm Sci, 2002 15: 115–133.

United States Pharmacopeia General Information chapter <1087> Apparent Intrinsic Dissolution-Dissolution Testing Procedures for Rotating Disc and Stationary Disc. In The United States Pharmacopeia and National Formulary USP 35–NF 30; The United States Pharmacopeial Convention, Inc.: Rockville, MD 2012; 660-663.

Yao Y, Lin G, Xie Y, Ma P, Li G, Meng Q, et al. Preformulation studies of myricetin: a natural antioxidant flavonoid. Pharmazie, 2014; 69: 19-26.

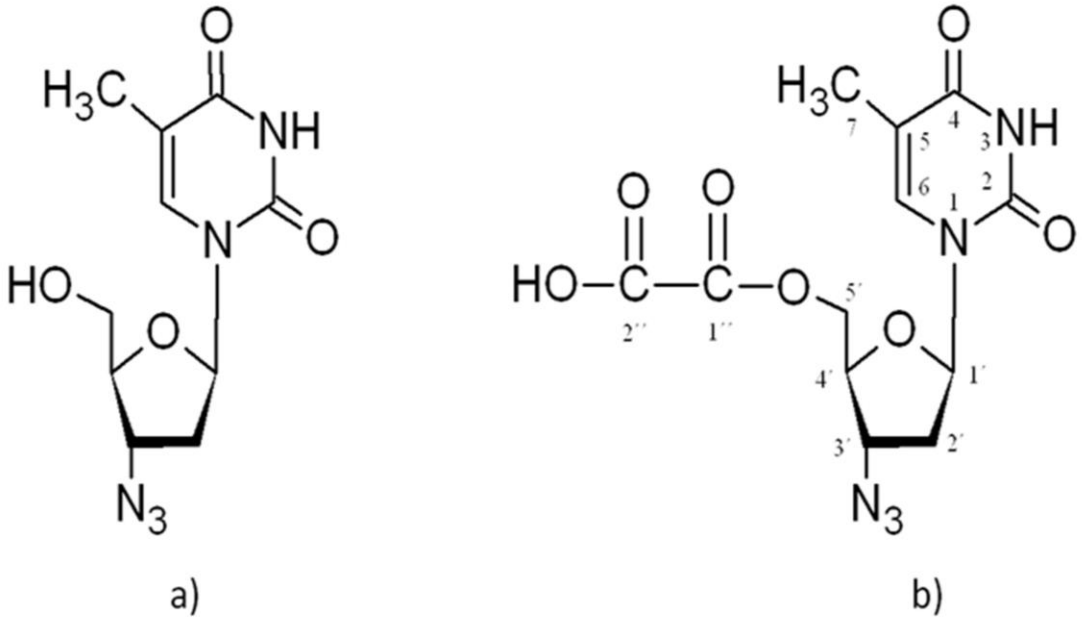

Figure 1. Chemical structures of (a) zidovudine (AZT) and (b) AZT-Ac, and atom numbering used in this study.

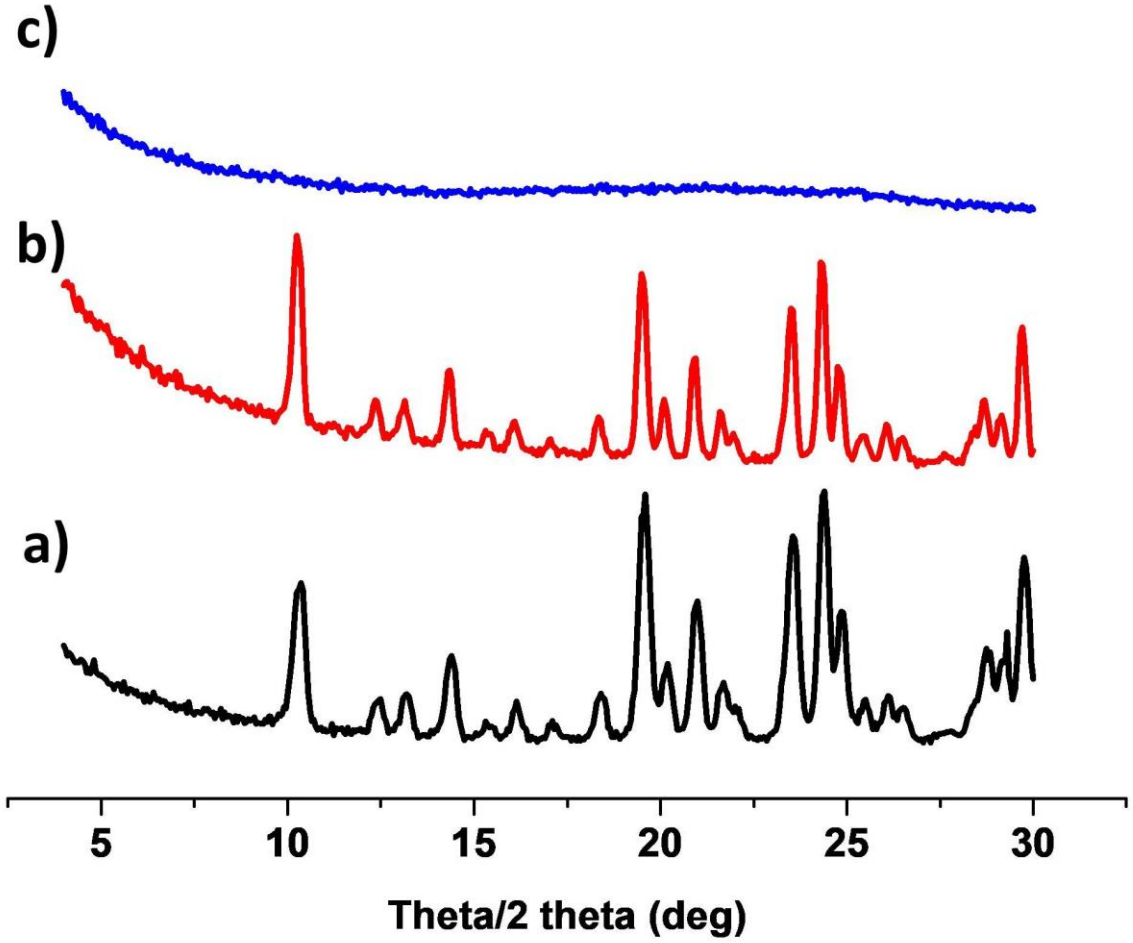

441

442 **Figure 2.** Overlay PXRD data for three representative samples of AZT-Ac. (a) AZT-Ac raw material; (b) AZT-
443 Ac-C (crystallized from acetonitrile), and (c) AZT-Ac-A (obtained by lyophilization from *t*-butanol-water, 20:80
444 v/v).

445

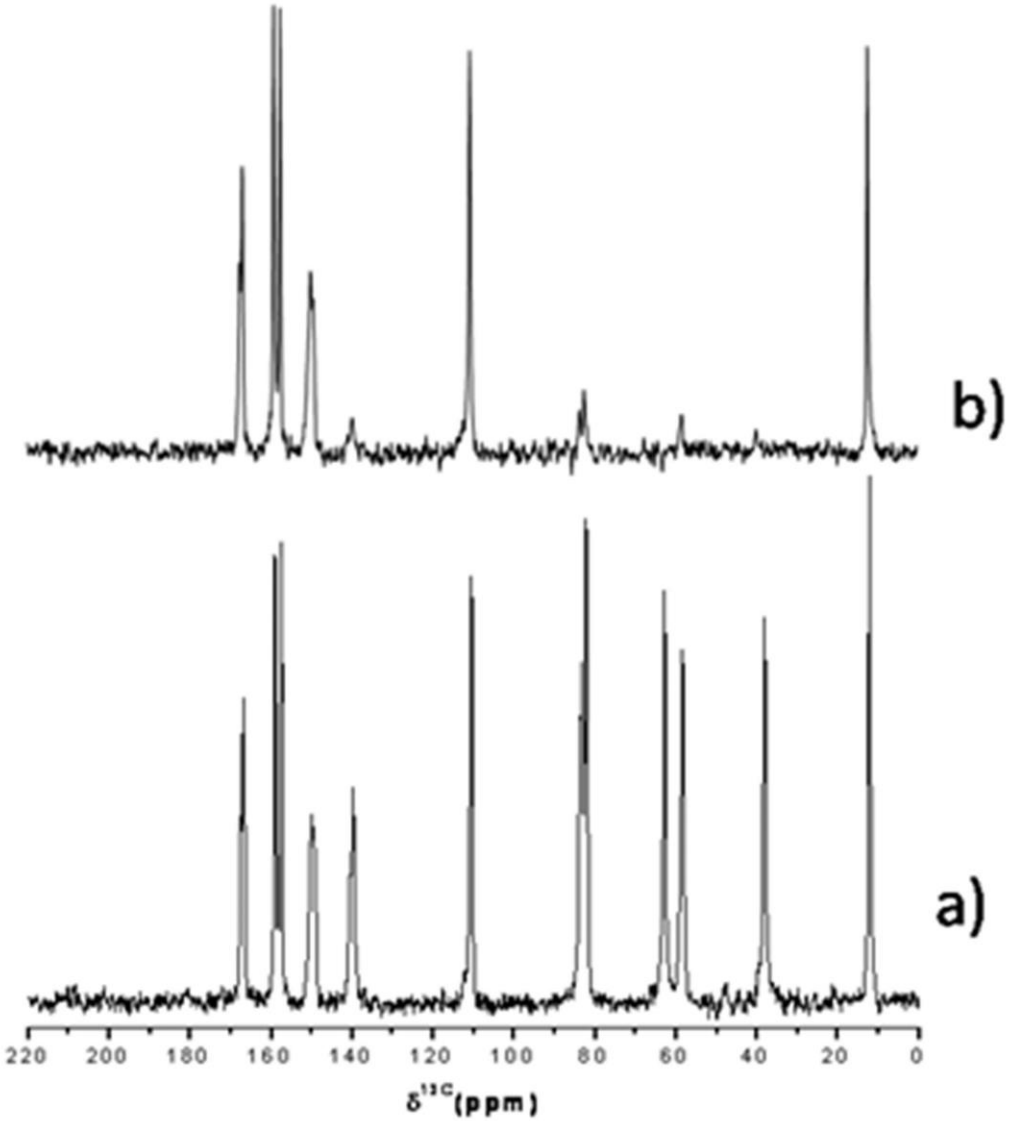

446

447 **Figure 3.** (a) SS ^{13}C NMR and (b) Non-Quaternary Suppression spectra of AZT-Ac-C.

448

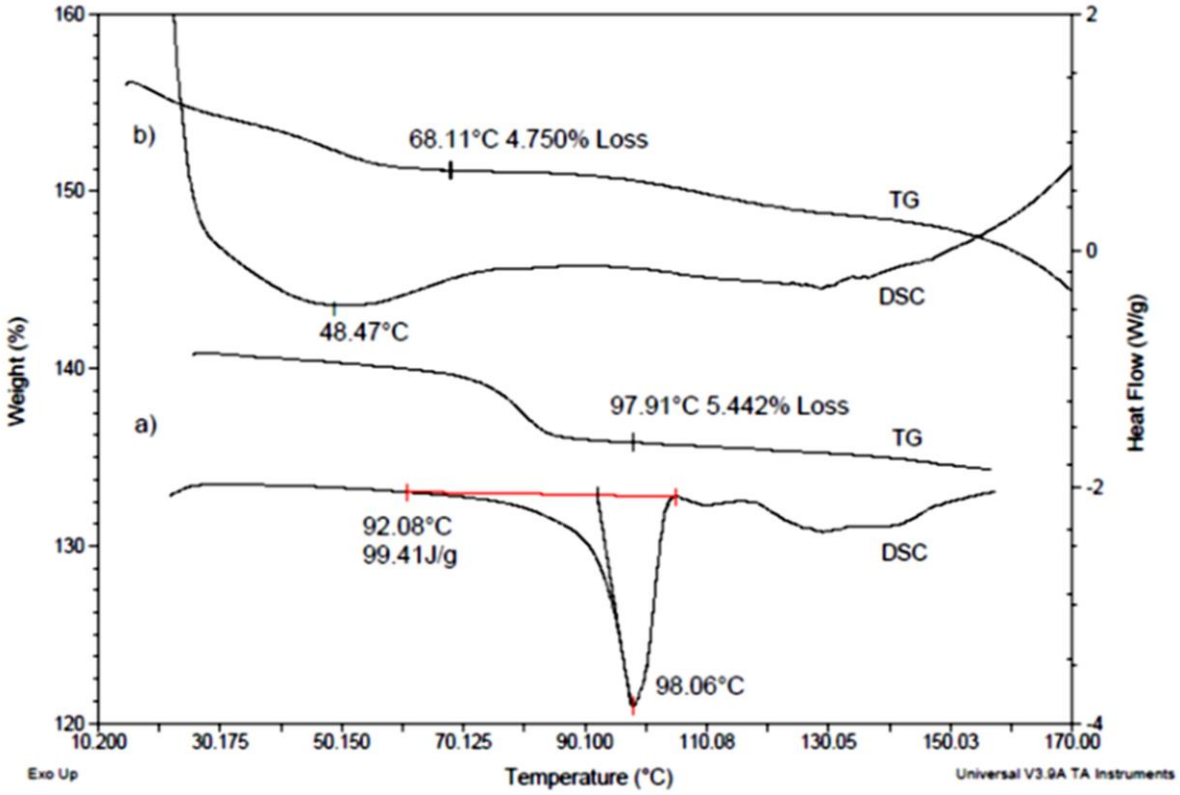

449

450

451 **Figure 4.** DSC (non-hermetically sealed pan) and TG (open pan) curves (10 °C/min, flowing N2 at 50 mL/min)

452 of: (a) AZT-Ac Form I and (b) AZT-Ac- A.

453

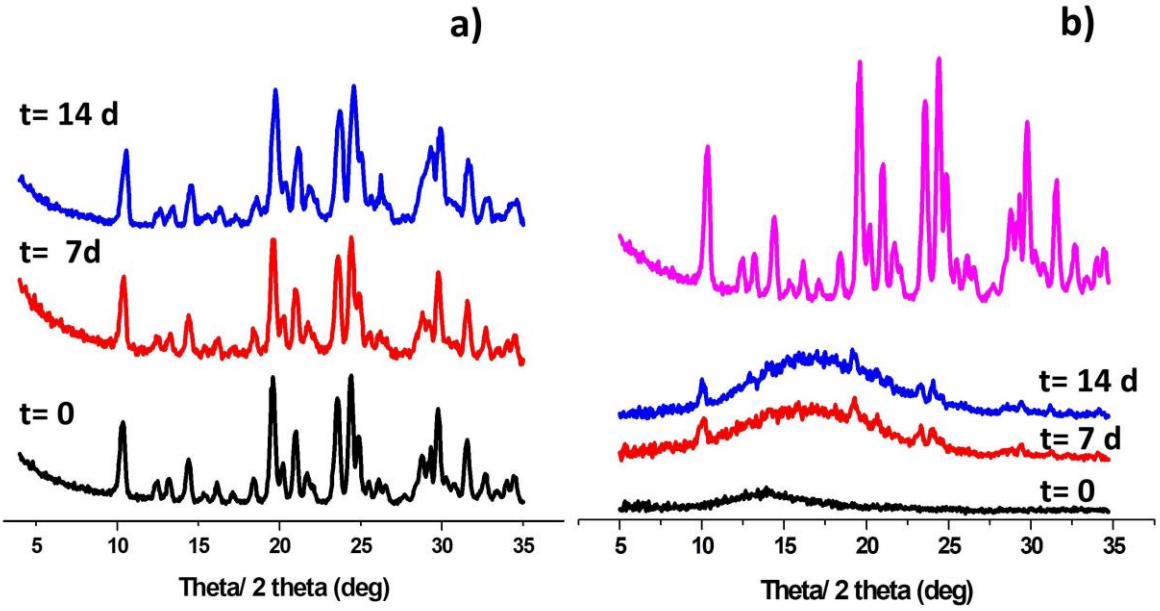

454

455 **Figure 5.** PXRD patterns of (a) AZT-Ac-C and (b) AZT-Ac-A after storage at 40°C/75% RH. To allow a

456 visual comparison, the powder pattern of AZT-Ac-C was included at the top of Figure 5b.

457

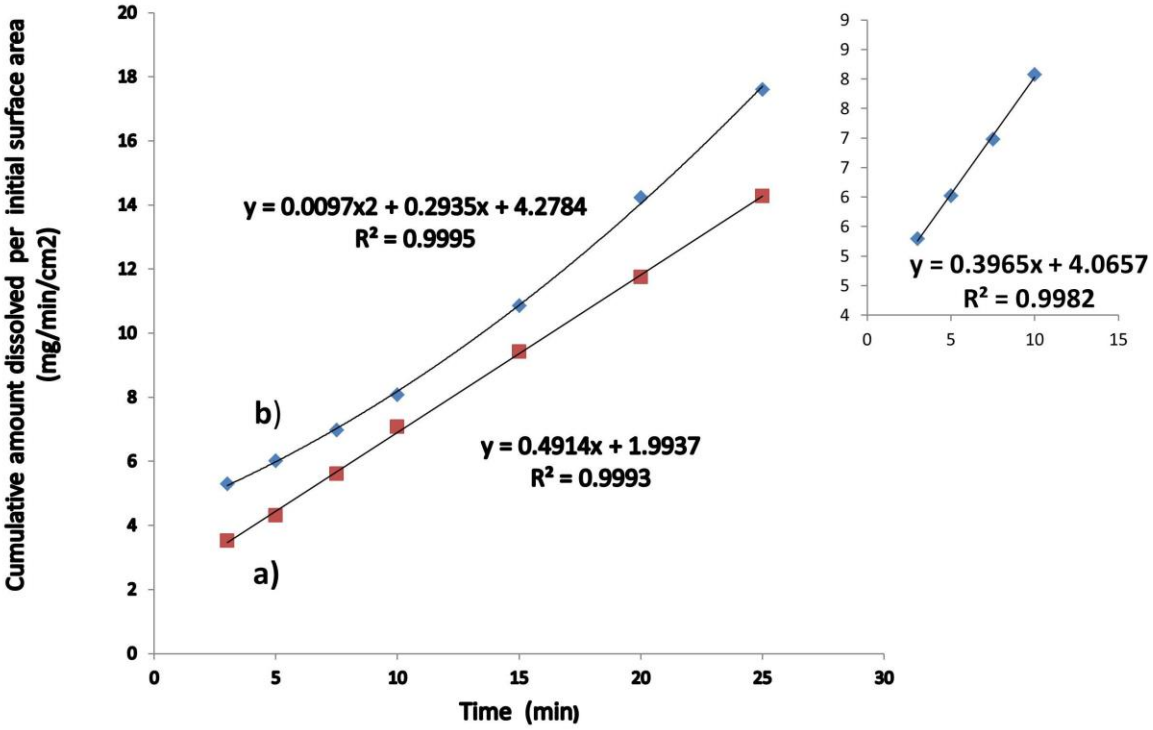

458

459 **Figure 6.** Disc Intrinsic dissolution profiles (50 rpm, 250 mL of degassed SGF, 37± 0.5 °C) of (a) AZT-Ac-C

460 and (b) AZT-Ac-A. Inset: linear portion of the intrinsic dissolution profile of AZT-Ac-A.

461